ELSEVIER

Contents lists available at ScienceDirect

Optics and Lasers in Engineering

journal homepage: www.elsevier.com/locate/optlaseng



Low-coherence snapshot phase-shifting diffraction phase microscope

Yuanyuan Sun¹, Yihan Wang¹, Daodang Wang^{*}, Stanley Pau, Rongguang Liang^{*}

James C. Wyant College of Optical Sciences, University of Arizona, 85721 Tucson, AZ, USA



ARTICLE INFO

Keywords:
Optical metrology
Quantitative phase imaging
Surface measurement
Optical testing

ABSTRACT

We proposed a Wollaston-prism-based snapshot phase-shifting diffraction phase microscope (WP-SPDPM) for low-coherence snapshot quantitative phase imaging and videography. Wollaston prism separates two orthogonally linearly polarized beams with high degrees of polarization at a sufficiently small separation angle; one of the beams passing through a pinhole serves as the reference beam. Four phase-shifted interferograms are simultaneously acquired with a polarization camera to accurately retrieve a high spatial resolution phase map. The system is nearly common-path in configuration and can achieve a large slope range and high accuracy. In addition to the ability to resist environmental noise, the WP-SPDPM is suitable for phase measurement using low-coherence light. The accuracy and large measurable slope range of the proposed system is validated and compared experimentally with a commercial profilometer. We believe WP-SPDPM is a powerful tool for the accurate and robust quantitative phase measurement and has a significant potential of the real-time phase imaging.

1. Introduction

The interferometric quantitative phase imaging (QPI) provides a powerful and accurate approach to characterizing the phase signature of a sample, and it has been widely applied in both optical metrology [1-3] and biomedical imaging [4,5]. The measured phase difference, which corresponds to the optical path difference between the test and reference beams, enables the evaluation of the profile or the refractive index distribution of the object under test. Likewise, the morphometric features of the cells and tissues, which are generally weakly scattering or transparent, can be precisely revealed under phase contrast measurement. Various interferometric QPI modalities, such as Hilbert phase microscope (HPM) [6,7], digital holography microscope (DHM) [8-10] and Fourier phase microscopy (FPM) [11,12], have been developed to achieve quantitative phase reconstruction. It is well known that traditional interferometric QPI systems are sensitive to environmental disturbances, such as mechanical vibration and air fluctuation, particularly in the non-common-path configuration or temporal phase shifting approach.

By combining common-path geometry and single-shot feature, the diffraction phase microscope (DPM) [13,14] provides an effective solution to greatly reduce the phase noise introduced by environmental disturbance. Most existing modalities with single-shot feature reconstruct the phase map using transform-based phase retrieval techniques, such as Fourier and Hilbert transforms, by which the snapshot measurement makes possible real-time metrology and biomedical imaging. However, due to the requirement of high spatial carrier frequency for informa-

tion separation in the frequency domain, which must be at least 3 times larger than spatial frequency bandwidth of tested sample, there is a limit to the amount of spatial information in the measurement, leading often to a partial loss of high frequency information in the reconstructed phase map. Additionally, phase retrieval based on a single interferogram is more vulnerable to environmental noise. In comparison, phase-shifting approach [15] provides an alternative way to reconstruct the phase map with both high spatial resolution and accuracy. In order to maintain the advantage of single-shot feature, a polarization-grating-based snapshot phase-shifting diffraction phase microscopy (SPDPM) was proposed by introducing the polarization property into the DPM [16]. It utilizes polarization grating to separate oppositely circularly polarized test and reference beams, by which four phase-shifted interferograms can be simultaneously obtained with a single shot using a polarization camera [17,18]. However, the high groove density in the polarization grating results in overly dense interference fringe, and a coherent laser source is required for illumination. Although folding mirrors could be added to the system to decrease the separation angle between the test and reference beams, the mirrors also increase system complexity and alignment difficulty.

In this paper, a Wollaston-prism-based snapshot phase-shifting diffraction phase microscope (WP-SPDPM) is proposed to achieve snapshot phase imaging and videography. Wollaston prism is used to separate orthogonally linearly polarized test and reference beams. Both beams are polarized with high degrees of polarization, and the system permits a sufficiently small separation angle between the test and reference arms. Four phase-shifted interferograms are acquired simultane-

^{*} Corresponding authors.

¹ These authors contributed equally to this work.

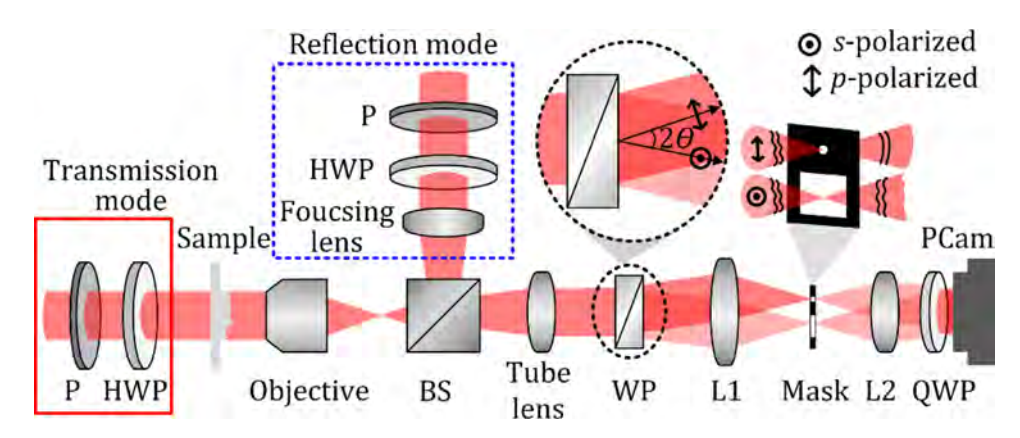


Fig. 1. System configuration of WP-SPDPM working in transmission and reflection modes: P, polarizer; HWP, half-wave plate; BS, beam splitter; WP, Wollaston prism; L1, L2, Lens; QWP, quarter-wave plate; PCam, polarization camera

ously in a single shot using a polarization camera. The sufficiently small separation angle between the test and reference arms makes the system nearly common path in configuration, significantly improving its ability to resist environmental noise and lowering the requirement on the coherence length of light source. Besides, it also increases the measurable phase slope range of tested object. The proposed WP-SPDPM has extremely fast acquisition speed as the existing DPM modalities limited by camera single frame rate, but with much higher spatial resolution and phase reconstruction accuracy due to its snapshot phase shifting mechanism. Section 2 presents the principle of the proposed Wollaston prismbased diffraction phase imaging method, including the system schematic configuration and the mathematic model based on Jones matrices and diffraction theory. Section 3 provides experimental measurement results of a 93-nm step height standard in the reflective mode and videography of dynamic evaporating alcohol droplets in the transmission mode demonstrate to illustrate both the high accuracy and measurable range of the proposed system. The polarization error analysis is discussed after. Finally, some concluding remarks are drawn in Section 4.

2. Principles and methods

2.1. System layout

The schematic configuration of the proposed WP-SPDPM is shown in Fig. 1. The system could be configured in both transmission (red solidboxed in Fig. 1) and reflection (blue dashed-boxed in Fig. 1) illumination modes. A compact low-coherence laser module (Thorlabs PL202, center wavelength $\lambda = 635$ nm, coherence length $L \sim 800$ µm) is employed as the light source in the system. The collimated beam with linear polarization reaches the tested sample and carries its phase information. And then, the sample is imaged on the plane at the Wollaston prism (WP) by the imaging optics consisting of an objective (Mitutoyo M Plan Apo 5× and NA 0.14) and a tube lens with focal length 105 mm. The WP splits the incident beam into two slightly off-axis beams with orthogonally linear polarization states, which travel to a 4f system consisting of an objective L1 (OLYMPUS PlanC N 10× and NA 0.25) and an achromatic doublet L2 with focal length 100 mm (Thorlabs AC254-100-AB-ML). A custom mask consisting of a pinhole and a large window is placed at intermediate Fourier plane of Lens L1. The s-polarized beam passes through the window and serves as the test beam with the carrying phase signature; the p-polarized beam travels towards the pinhole to obtain the diffraction wave serving as reference wave. A quarter-wave plate QWP (BOV AQWP3) with its fast axis orientated at 45° relative to the linear polarization orientation is used to transform the orthogonally linearly polarized test and reference beams to be oppositely circularly polarized. Snapshot phase shifting is implemented by utilizing a microgrid monochromatic polarization camera (Blackfly S USB3 BFS-U3-51S5P-C, resolution: 2448 \times 2048, pixel size: 3.45 μ m, frame rate: 75 fps) to extract the phase signature of the tested sample within the field-of-view (FOV) of 380 μ m \times 320 μ m. A cubic interpolation algorithm is adopted to avoid spatial resolution loss and reduce the instantaneous field-of-view (IFOV) error for microgrid polarization camera. To increase the polarization quality, a polarizer with fast axis parallel to the laser polarization orientation is utilized after the laser source. By rotating the fast axis of a half-wave plate (HWP) placed after the polarizer, the relative intensity of interfering waves can be adjusted to obtain the ideal fringe contrast without losing total flux.

As employing the WP to separate the test and reference beams as shown in Fig. 1, the two orthogonally linearly polarized beams with extinction ratio higher than 104 can be obtained to ensure high degree of linear polarization after WP and accurate circular polarizability after QWP; thus, high phase retrieval accuracy can be achieved with polarization phase-shifting method. In addition, the proposed WP-SPDPM has three unique features. The first is that the system is nearly commonpath in configuration with a sufficiently small separation angle of $\sim 1^{\circ}$ between the two interfering waves, which is far smaller than the typical value of a polarization grating of $\sim 5^{\circ}$ [16,19]; thus, its ability to resist environmental noise can be significantly improved and the measurable height and slope range can be effectively increased. The second feature is that it places low requirement on the coherence length of light source, potentially suitable for phase measurement with lowcoherence light. Another notable feature is that only one frame capture is needed to get all four $\pi/2$ phase-shifted interferograms simultaneously. The proposed system is fast and insensitive to environmental disturbance.

Although low-coherence source is used in the system, whose coherence length is far smaller than that of a traditional He-Ne laser (Coherence length > 20 cm), there remains small amount of spurious fringes introduced by the laser and optical elements in the system. A straightforward solution to mitigate such spurious interference is background removal. The null testing, that is with no tested sample in transmission mode and with a reference mirror as tested sample in reflection mode, can be performed to acquire the background phase images, and then they can be subtracted from the acquired testing phase images of the tested sample. Background removal also removes the small wavefront tilt due to the separation angle between the test and reference beams, including the corresponding related high-order aberrations.

2.2. Mathematic model

The proposed WP-SPDPM can be modelled using Jones matrices and diffraction theory. The Jones matrices describe the polarization changes through the polarization elements, and diffraction theory models the low-pass spatial filtering process through the pinhole. Both the test and reference arms start with a linearly polarized beam E_{in} orientated at angle α with the tested sample phase information $\varphi_s(x, y)$. The eigenpolarization states of the WP are horizontally and vertically linearly polarized. The electric field E_{test} of the test beam after passing through WP

and QWP can be described as

$$\begin{split} E_{test} &= J_{QWP} \cdot J_{WP}^{test} \cdot E_{in} \\ &= \frac{1}{\sqrt{2}} \begin{bmatrix} 1 & -i \\ -i & 1 \end{bmatrix} \begin{bmatrix} e^{ik\theta x} & 0 \\ 0 & 0 \end{bmatrix} \begin{bmatrix} \cos \alpha \\ \sin \alpha \end{bmatrix} e^{i\varphi_s(x,y)} \\ &= \frac{\cos \alpha}{\sqrt{2}} e^{i[k\theta x + \varphi_s(x,y)]} \begin{bmatrix} 1 \\ -i \end{bmatrix}, \end{split} \tag{1}$$

where J_{WP}^{test} and J_{QWP} are the Jones matrices for the WP on test arm and QWP, respectively, and θ is the half separation angle between the propagating directions of different polarized beams existing from the WP. The reference beam E_{ref} can be described as

$$\begin{split} E_{ref} &= J_{QWP} \cdot \mathcal{F}^{-1} \left\{ \mathcal{F} \left\{ J_{WP}^{ref} \cdot E_{in} \right\} \cdot \delta(\xi - \theta/\lambda) \right\} \\ &= \frac{1}{\sqrt{2}} \begin{bmatrix} 1 & -i \\ -i & 1 \end{bmatrix} \\ &\cdot \mathcal{F}^{-1} \left\{ \mathcal{F} \left\{ \begin{bmatrix} 0 & 0 \\ 0 & e^{-ik\theta x} \end{bmatrix} \cdot \begin{bmatrix} \cos \alpha \\ \sin \alpha \end{bmatrix} e^{i\varphi_s(x,y)} \right\} \cdot \delta(\xi - \theta/\lambda) \right\} \\ &= \frac{\Phi(0,0) \sin \alpha}{\sqrt{2}} e^{-ik\theta x} \begin{bmatrix} -i \\ 1 \end{bmatrix}, \end{split} \tag{2}$$

where J_{WP}^{ref} is the Jones matrix for the WP on reference arm and $\mathcal{F}\{e^{i\varphi_s(x,y)}\}=\Phi(\xi,\eta)$ denotes the Fourier pattern of the sample phase under test. In Eq. (2), the pinhole on the mask is modeled as a delta function $\delta(\xi)$ and it low-pass filters the high-frequency information and only leaves the constant term $\Phi(0,0)$. For the interfering test and reference beams after passing through the micro-polarizer array on polarization camera sensor, we have the acquired intensity

$$\begin{split} I_{pol} &= \left| J_{LP}^{pol} \cdot \left(E_{test} + E_{ref} \right) \right|^2 \\ &= I_{DC} - I_{AC} \sin \left[2k\theta x + \varphi_s(x, y) + \frac{\pi}{2} \cdot \frac{pol}{45^{\circ}} \right], \end{split} \tag{3}$$

where J_{LP}^{pol} denotes the Jones matrix for the linear micro-polarizer with transmission axis oriented at the angle pol, $pol \in \{0^\circ, 45^\circ, 90^\circ, 135^\circ\}$ the direct current term $I_{DC} = (\cos^2\alpha + \Phi^2(0,0)\sin^2\alpha)/2$ and the alternating current term $I_{AC} = \sin 2\alpha \ \Phi(0,0)/2$. Thus, the phase signature $\varphi_s(x,y)$ of tested sample can be obtained with the four-step phase shifting algorithm,

$$\varphi_s = \tan^{-1} \left(\frac{I_{45^{\circ}} - I_{135^{\circ}}}{I_{0^{\circ}} - I_{90^{\circ}}} \right). \tag{4}$$

The maximum local phase difference between two adjacent reconstruction pixels is required to be less than π ; otherwise, there is a 2π ambiguity in the phase calculation. A smaller separation angle between the test and reference beams allows a larger measurable local phase contribution from tested sample. The maximum measurable local phase change between two adjacent pixels $\Delta \phi_{total} \leq \pi$ is

$$\Delta\varphi_{total} = \frac{2\pi}{\lambda} \cdot 2\theta' \cdot \Delta x_{pixel} + \Delta\varphi_s, \tag{5}$$

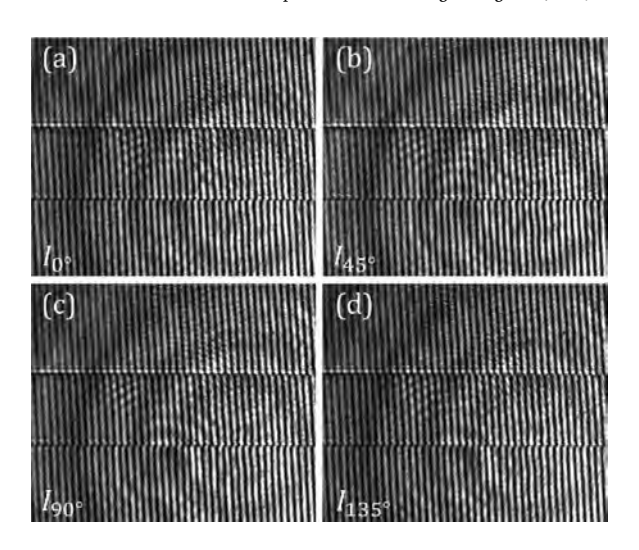


Fig. 2. Acquired interferograms in the testing of a step height sample with the proposed WP-SPDPM: (a) 0° , (b) 45° , (c) 90° and (d) 135° .

where Δx_{pixel} is the pixel size of the sensor, $\Delta \varphi_s$ is the local phase signature from tested sample corresponding to two adjacent pixels, and 2θ ' indicates the separation angle between the reference and test beams on the sensor. Thus, the maximum measurable surface slope in the proposed WP-SPDPM was calculated to be over 60° at the operating wavelength $\lambda=635$ nm under the lateral resolution $\Delta x=0.156~\mu m$ of the system. The measurable local slope range can be further increased either by improving the lateral resolution or by employing an illumination wave with a longer wavelength.

3. Experimental results and analysis

3.1. Step height standard

To demonstrate the feasibility and accuracy of the proposed WP-SPDPM, a reflective 93-nm step height standard (VLSI, KTS-1800 QS) was measured with the proposed system. The simultaneously acquired four phase-shifted interferograms with four different phase shifts are shown in Fig. 2. According to Fig. 2, some inherent spurious fringes could be observed in the acquired interferograms, and background removal is performed to remove these spurious fringes. Fig. 3(a) and 3(b) shows reconstructed phase maps before and after background removal. It can be seen from Fig. 3 that a smoother phase is obtained after removing the irregular circular disturbances brought by the laser source.

The reconstructed surface of the tested step height standard measured by the WP-SPDPM is shown in Fig. 4(b), from which a smooth surface and a sharp step edge can be seen. According to Fig. 4(b), the

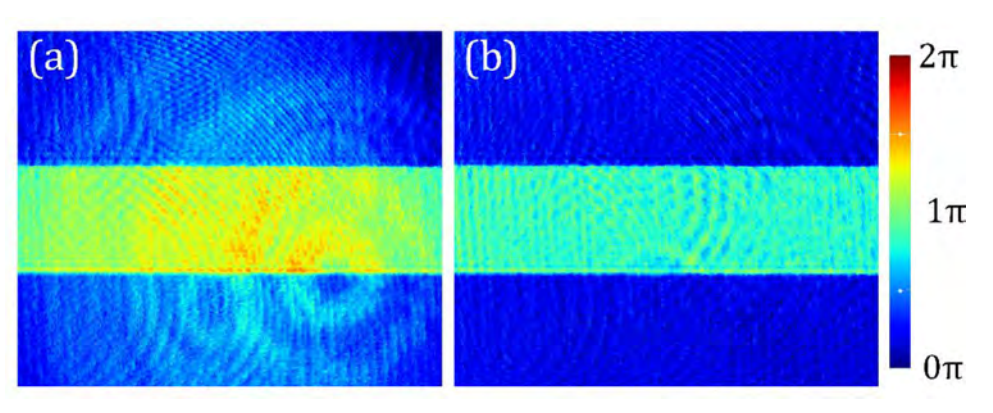


Fig. 3. Reconstructed phases in the testing of a step height sample: (a) before and (b) after background removal.

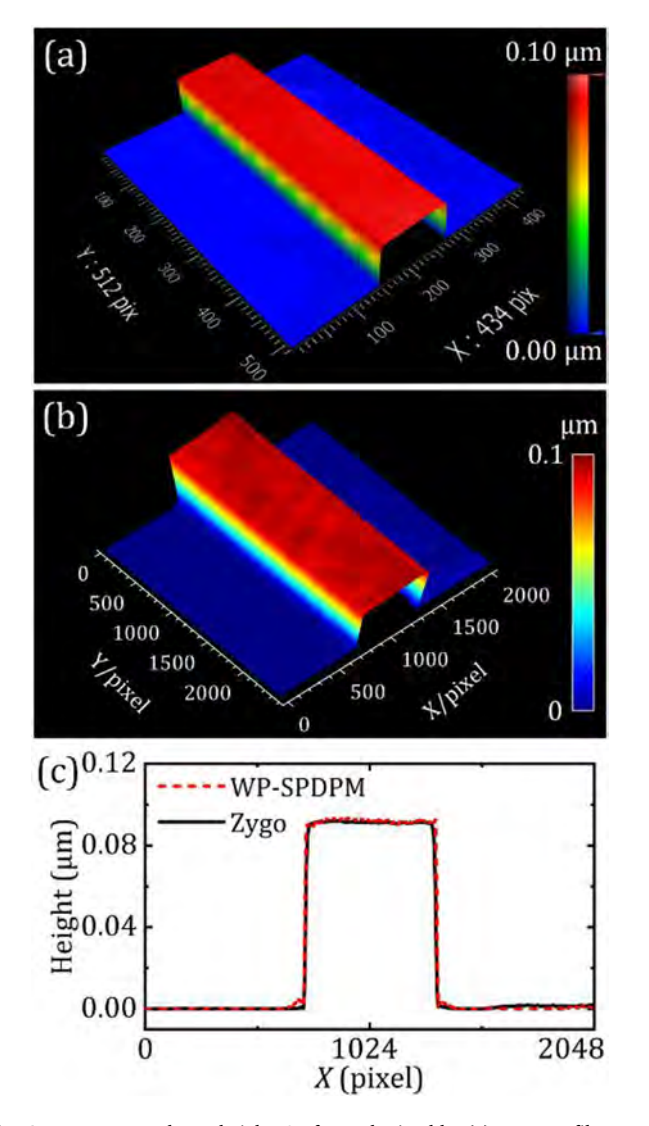


Fig. 4. Reconstructed step height. Surfaces obtained by (a) Zygo profilometer, (b) WP-SPDPM, and (c) line profile comparison.

measured average step height is 93.47 nm, with the deviation from nominal value being 0.47 nm. For comparison, the same step has also been measured with a Zygo NewView 8300 optical surface profiler, and the obtained surface profile is shown in Fig. 4(a). The line profiles comparison of the measured step height with the proposed WP-SPDPM and Zygo profilometer is given in Fig. 4(c). According to Fig. 4, the measured step height with Zygo profilometer is 92.88 nm, with the corresponding difference being about 0.6 nm between the proposed WP-SPDPM result and that of Zygo profilometer; thus, a good agreement is achieved in the measurement. The measured surface root mean square (RMS) error is 5.31 nm for the WP-SPDPM and 0.91 nm for the Zygo profilometer. The deviation is mainly caused by the coherence noise of the laser source. Either a lower coherence source or a light diffuser can be used to further reduce the noise of the WP-SPDPM.

3.2. Dynamic alcohol droplets

To verify the large measurable height range and slope dynamic range of the WP-SPDPM, the phase measurements of alcohol droplets with different shapes were separately characterized. The alcohol solution was sprayed on a glass substrate, and the corresponding phase signature was measured. The surface profiles of the alcohol droplets were estimated assuming a refractive index of 1.3614. Due to the snapshot feature of WP-SPDPM, the change of the alcohol droplets during evaporation process can be recorded with the proposed system in real time, i.e., real-time phase video graphing. The interferograms during evaporation process were recorded at the frame rate 50 fps to observe profile changes (Visualization 1 and Visualization 2) of two droplets of different sizes. Fig. 5(a-c) present the reconstructed 3D profiles of the gradually decreasing edge slope of a larger droplet during the evaporation process, with the maximum peak-to-valley value of 47.58 μ m. The maximum local slope in Fig. 5(a) are 9.29° Fig. 5(d-f) provide the reconstructed 3D profiles of the process by which several small alcohol droplets were evaporated within 1 second. The largest peak-to-valley value in Fig. 5(d) is 7.00 μ m with maximum local slope of 13.43° According to Fig. 5(a-f), both large measurable height range and slope range can be achieved by the proposed WP-SPDPM.

3.3. Polarization error analysis

Owing to the imperfection of the microgrid polarization camera and system alignment, there exists certain polarization errors from different sources. The main error sources include camera instantaneous field-

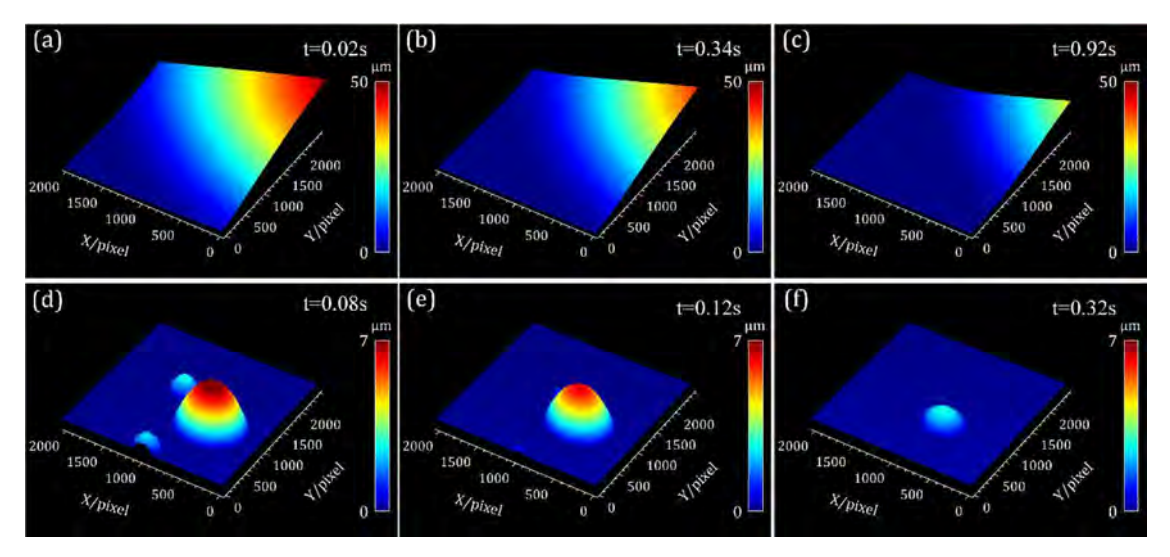


Fig. 5. Reconstructed surface profiles of two droplets evaporating process. Surface profiles of (a-c) a large droplet and (d-f) a small droplet.

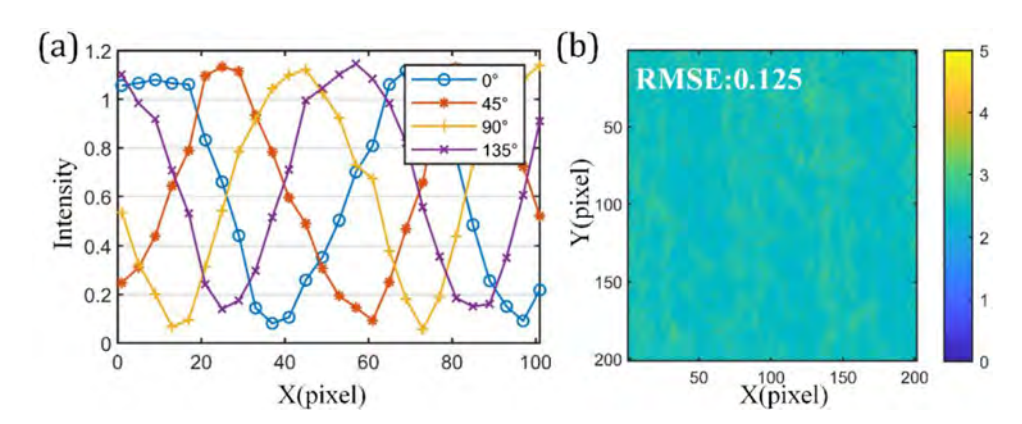


Fig. 6. (a) Line profile of the four phase shifted images of the real measurement. (b) The superposition of the four phase shifted images of the real measurement.

of-view (IFOV) error, QWP orientation misalignment, wavelength mismatch between the laser and the QWP and the linear polarization imperfection of the WP. Based on the specification of the utilized QWP and WP, the phase error introduced by WP polarization imperfection and QWP wavelength mismatch can be approximately estimated. The extinction ratio of the WP reaches to 10⁴. Without considering other error sources, the maximum phase error is less than 0.0032λ . It indicates that the high polarization performance of WP greatly minimizes the phase error from polarization imperfection. Besides, the QWP utilized in the proposed system is a broadband achromatic retarder whose retardance at 635 nm is approximately 0.5018π . Under this scenario, the introduced phase error is limited to $1.27 \times 10^{-6} \lambda$, which is negligible. According to existing research [15,16], the orientation misalignment of QWP as well as IFOV error from microgrid polarization camera will lead to intensity variations and phase shift deviations in different polarizations channels. Consequently, the superposition of the four phase shifted images $I_{0^{\circ}}+I_{45^{\circ}}+I_{90^{\circ}}+I_{135^{\circ}}$ would have severe stripe patterns. To make sure the IFOV error and QWP orientation misalignment were not dominant in our system, the real measured line profiles and the superposition of four phase images from step height standard measurement were checked and demonstrated in Fig 6. As shown in Fig. 6(a), the line profiles of four polarization channels have uniform amplitude and modulation without obvious intensity or phase variations. The superposition map in Fig. 6(b) appears uniform without stripe patterns, indicating that the QWP misalignment error and IFOV error is minimal in the proposed system.

4. Conclusion

In conclusion, the proposed WP-SPDPM enables the accurate quantitative phase imaging and videography with both large slope dynamic range and high spatial resolution in real-time. The system can be easily setup in both transmission and reflection illumination modes to measure a broad range of samples with different surface characteristics. The nearly-common-path configuration of the proposed system minimizes the effects of environmental disturbance, and the low-coherence source reduces the coherence noise in the measurement. Both the high accuracy and a large slope dynamic range have been validated and compared with measurements using a commercial profilometer. It provides a powerful tool for the accurate and robust quantitative phase measurement with a large slope dynamic range and high spatial resolution, and also has a significant potential of the real-time phase imaging.

Funding

This work is supported by National Science Foundation (1918260, 2034210, 2053754); and National Institutes of Health (S100D018061).

Declaration of Competing Interest

The authors declare that they have no known competing financial interests or personal relationships that could have appeared to influence the work reported in this paper

CRediT authorship contribution statement

Yuanyuan Sun: Methodology, Validation, Writing – original draft. Yihan Wang: Software, Validation, Writing – original draft. Daodang Wang: Conceptualization, Supervision. Stanley Pau: Conceptualization, Writing – original draft, Supervision. Rongguang Liang: Conceptualization, Supervision.

Data availability

Data underlying the results presented in this paper are not publicly available at this time but may be obtained from the authors upon reasonable request.

References

- Zhou R, Edwards C, Popescu G, Goddard L. Semiconductor defect metrology using laser-based quantitative phase imaging. SPIE 2015:146–51.
- [2] de Groot PJ. A review of selected topics in interferometric optical metrology. Rep Progr Phys 2019;82:056101.
- [3] Marrugo AG, Gao F, Zhang S. State-of-the-art active optical techniques for three-dimensional surface metrology: a review [Invited]. J Opt Soc Am A 2020;37:B60–77.
- [4] Popescu G. Quantitative phase imaging of cells and tissues. McGraw-Hill Education; 2011.
- [5] Park Y, Depeursinge C, Popescu G. Quantitative phase imaging in biomedicine. Nat Photonics 2018;12:578–89.
- [6] Ikeda T, Popescu G, Dasari RR, Feld MS. Hilbert phase microscopy for investigating fast dynamics in transparent systems. Opt Lett 2005;30:1165–7.
- [7] Gabriel P, Takahiro I, Catherine B, Kamran B, Ramachandra RD, Michael SF. Erythrocyte structure and dynamics quantified by Hilbert phase microscopy. J Biomed Opt 2005;10:060503.
- [8] Myung KK. Principles and techniques of digital holographic microscopy. SPIE Rev 2010;1:018005.
- [9] Rappaz B, Marquet P, Cuche E, Emery Y, Depeursinge C, Magistretti PJ. Measurement of the integral refractive index and dynamic cell morphometry of living cells with digital holographic microscopy. Opt Express 2005;13:9361–73.
- [10] Marquet P, Rappaz B, Magistretti PJ, Cuche E, Emery Y, Colomb T, Depeursinge C. Digital holographic microscopy: a noninvasive contrast imaging technique allowing quantitative visualization of living cells with subwavelength axial accuracy. Opt Lett 2005;30:468–70.
- [11] Lue N, Choi W, Popescu G, Ikeda T, Dasari RR, Badizadegan K, Feld MS. Quantitative phase imaging of live cells using fast Fourier phase microscopy. Appl Opt 2007:46:1836–42.
- [12] Popescu G, Deflores LP, Vaughan JC, Badizadegan K, Iwai H, Dasari RR, Feld MS. Fourier phase microscopy for investigation of biological structures and dynamics. Opt Lett 2004;29:2503–5.
- [13] Bhaduri B, Edwards C, Pham H, Zhou R, Nguyen TH, Goddard LL, Popescu G. Diffraction phase microscopy: principles and applications in materials and life sciences. Adv Opt Photon 2014;6:57–119.
- [14] Popescu G, Ikeda T, Dasari RR, Feld MS. Diffraction phase microscopy for quantifying cell structure and dynamics. Opt Lett 2006;31:775–7.

- [15] Hariharan P, Oreb BF, Eiju T. Digital phase-shifting interferometry: a simple error-compensating phase calculation algorithm. Appl Opt 1987;26:2504-6.
 [16] Tian X, Liang R. Snapshot phase-shifting diffraction phase microscope. Opt Lett 2020;45:3208-11.
- [17] Millerd JE, Brock NJ, Hayes JB, North-Morris MB, Novak M, Wyant JC. Pixelated phase-mask dynamic interferometer. In: Proceedings of SPIE 5531, interferometry XII: techniques and analysis; 2004. p. 304–14.
- [18] Tian X, Tu X, Della Croce K, Yao G, Cai H, Brock N, Pau S, Liang R. Multi--wavelength quantitative polarization and phase microscope. Biomed Opt Express 2019;10:1638–48.
- Z019;10:1638–48.
 [19] Chen W, Zhao Z, Wang C, Li H, Wei R, Zhang S, Peng Z, Liu Y, Wang Q, Mu Q. Linear polarization grating combining a circular polarization grating with a special cycloidal diffractive quarter waveplate. Opt Express 2019;27: 33378–33390.